PAPER

Stainless steel made to rust: a robust water-splitting catalyst with benchmark characteristics†

Helmut Schäfer,*[a] Shamaila Sadaf,[a] Lorenz Walder,[a] Karsten Kuepper,[b] Stephan Dinklage,[c] Joachim Wollschläger,[b] Lilli Schneider,[b] Martin Steinhart,[a] Jörg Hardege[d] and Diemo Daum[c]

The oxygen evolution reaction (OER) is known as the efficiency-limiting step for the electrochemical cleavage of water mainly due to the large overpotentials commonly used materials on the anode side cause. Since Ni–Fe oxides reduce overpotentials occurring in the OER dramatically they are regarded as anode materials of choice for the electrocatalytically driven water-splitting reaction. We herewith show that a straightforward surface modification carried out with AISI 304, a general purpose austenitic stainless steel, very likely, based upon a dissolution mechanism, to result in the formation of an ultra-thin layer consisting of Ni, Fe oxide with a purity >99%. The Ni enriched thin layer firmly attached to the steel substrate is responsible for the unusual highly efficient anodic conversion of water into oxygen as demonstrated by the low overpotential of 212 mV at 12 mA cm^{-2} current density in 1 M KOH, 269.2 mV at 10 mA cm^{-2} current density in 0.1 M KOH respectively. The Ni, Fe-oxide layer formed on the steel creates a stable outer sphere, and the surface oxidized steel samples proved to be inert against longer operating times (>150 ks) in alkaline medium. In addition Faradaic efficiency measurements performed through chronopotentiometry revealed a charge to oxygen conversion close to 100%, thus underpinning the conclusion that no "inner oxidation" based on further oxidation of the metal matrix below the oxide layer occurs. These key figures achieved with an almost unrivalled-inexpensive and unrivalled-accessible material, are among the best ever presented activity characteristics for the anodic water-splitting reaction at pH 13.

Introduction

Solar energy can be captured and stored in the form of chemical bonds to provide solar fuels (artificial storage of solar energy).[1–3] Photochemical or electrochemical cleavage of water into hydrogen and oxygen, particularly when realized using renewable energy sources, potentially presents an attractive solar to fuel conversion route. In the water-splitting process the anode side at which the oxygen evolution reaction (OER) takes place, still requires optimization, because the anode causes the majority of the total

overpotential of a system consisting of established electrode materials. For technical reasons a reasonable current density of around 10 mA cm^{-2} should be guaranteed at potentials being close to 1.228 V *versus* the reversible hydrogen electrode (RHE). Noble metal oxides like IrO$_2$ and RuO$_2$ which are well known for their water-splitting characteristics fulfil these requirements[4–12] but are expensive and more over do not exhibit marked long term stability in alkaline water electrolysis conditions.[13] MnO$_x$ compounds lend themselves as water-splitting catalysts[14–17] but generally show low electrocatalytic efficiency. Very recently Ni–Fe oxide/hydroxides[18–20,22] underwent a renaissance and showed considerable catalytic performance in case of Ni$_x$Fe$_y$O$_z$ nanoparticles[21] as well as in case of electrodeposited thin films consisting of Ni$_x$Fe$_y$O$_z$[20] and Ni$_x$Fe$_y$(OH)$_2$.[22] We show that both catalytic active metal centres (Ni, Fe) of these advanced materials are ingredients of stainless steels such as AISI 304 steel, AISI 316 steel, AISI 316L steel that are commonly available, non-toxic, cost effective materials ideal for water-splitting catalysis.

Different metals and metal alloys including steel have been studied as prospective catalysts for the electrocatalytic OER above all in alkaline medium over the past decades.[2,12,23–32] However, to the best of our knowledge no significant OER below 400 mV

[a] *Institute of Chemistry of New Materials and Center of Physics and Chemistry of New Materials, Universität Osnabrück, Barbarastrasse 7, 49076 Osnabrück, Germany. E-mail: helmut.schaefer@uos.de*

[b] *Fachbereich Physik, Universität Osnabrück, Barbarastrasse 7, 49076 Osnabrück, Germany*

[c] *Fakultät Agrarwissenschaften und Landschaftsarchitektur, Labor für Pflanzenernährung und Chemie, Hochschule Osnabrück, Am Krümpel 31, 49090 Osnabrück, Germany*

[d] *School of Biological, Biomedical and Environmental Sciences, University of Hull, Cottingham Road, Hull, HU6 7RX, UK*

† Electronic supplementary information (ESI) available. See DOI: 10.1039/c5ee01601k

This journal is © The Royal Society of Chemistry 2015

Energy Environ. Sci., 2015, **8**, 2685–2697 | 2685

Paper

Table 1 Overview of the performed surface oxidations and the comparison samples IrO_2–RuO_2, AISI 304, Ni42 and iron. The overpotential was determined at a current density of 10 mA cm^{-2} without compensation of the voltage drop. The anodization was performed at an average potential difference of 5.2 V between working- and CE and a current density of 1.77 A cm^{-2} (Elox fix) in 7.2 M NaOH in case of samples Elox300 and Elox480. Cyclic oxidation (Elox cycl) was performed (sample EloxCycl) in 1.5 M NaOH between 1 and 2.25 V against RHE; the maximum current amounted to 1 A due to device limitations and the maximum current density amounted to 294 mA cm^{-2}

Sample	Way of oxidation	Temperature (K)	Duration (min)	Overpotential in 0.1 M KOH (mV)
Iron	No oxidation	—	—	510
IrO_2–RuO_2	No oxidation	—	—	452
AISI304	No oxidation	—	—	465
Ni42	No oxidation	—	—	347
Elox300	Elox fix 300	323	300	269.2
Elox480	Elox fix 480	323	480	292.0
EloxCycl	Elox cycl	323	^{a}	395

^{a} Number of cycles: 500.

overpotential in diluted alkaline regime was reported in protocols up to now[26,28,29] proving the overall moderate electro catalytic properties far below of up to date benchmark species. We were curious if for instance *via* dissolution–, dissolution–precipitation or electromigration processes on AISI 304 steel the chromium content at the periphery of the alloy can be suppressed so that a high-purity bimetallic (Ni, Fe) oxide (or hydroxide) containing slim film that is firmly attached to the metal matrix can be established rendering the responsible steel surface in an ideal case as active, as the highly advanced pure Ni, Fe species previously mentioned.

Hard anodization (oxidation) performed in strong alkaline medium at current densities of almost 1800 mA cm^{-2} of the surface was performed to cope with this challenging task (Table 1 and Fig. S1, ESI,† details see Experimental section).

Results and discussion

Table 1 gives an overview of the prepared samples Elox300, Elox480, EloxCycl, respectively the comparison samples, iron (>99.9% grade), Ni42 (alloy made of untreated AISI Ni42), IrO_2–RuO_2 (IrO_2/RuO_2 coated titanium) as well as AISI304 (untreated AISI 304 reference sample). The performed oxidation procedures were indicated by "Elox fix 300" for 300 min of electro-activation leading to sample Elox300, respectively by "Elox fix 480" for 480 min electro activation leading to sample Elox480 and "Elox cycl" for activation *via* repetitive potential cycling leading to sample EloxCycl. Each of the sample preparation was repeated seven times (EloxCycl: two times).

The effectiveness of the electro oxidation of metals performed in alkaline medium to heighten the electrode performance was shown by different groups.[12,28–31] However a targeted increase of the electrocatalytic OER properties of AISI 3XX steel types upon this specific activation procedure has to the best of our knowledge not been shown so far. The major difference between our electro oxidation process and the already established procedures are the considerably harsher conditions of our treatment, performed in

7.2 molar NaOH at 50 °C and at current densities of 1770 mA cm^{-2} for 300 min (sample Elox300) respectively 480 min (sample Elox480) (Table 1). Our best result (sample Elox300) could be achieved after 5 hours activation at a constant voltage of 5.2 V (current 5.3 A, T = 323 K) between sample and counter electrode (CE) (Fig. 1a and b and Fig. S1, ESI†). Sample Elox300 showed afterwards besides an amazing stability at constant current (Fig. 1b) even after tens of hours operating time at 10 mA cm^{-2} in addition an extremely strong voltage–current behaviour (average overpotential for the OER: 269.2 mV at 10 mA cm^{-2} in 0.1 M KOH (Fig. 1a and b)). An overpotential of only ∼212 mV at 12 mA cm^{-2} could be detected in 1 M KOH (Fig. S2, ESI†). Current densities of the oxidized samples like *e.g.* Elox300 at specific potentials derived from cyclic voltammograms (CVs) (Fig. 1a: 10 mA cm^{-2} at 276 mV overpotential) can be well translated into non steady state data, *e.g.* log-term chronopotentiometry data (Fig. 1b: 269.2 mV overpotential at 10 mA cm^{-2}). It should be mentioned at this point that all electrochemical measurements have been carried out without any correction of a voltage drop.

The oxide layer obviously provides a stable periphery, *i.e.* stabilizes the sample outwardly: sample Elox300 showed no weight loss even after longer operating times (>50 000 s chronopotentiometry at 10 mA cm^{-2} in 0.1 M KOH, Table S1, ESI†) and an analysis of the electrolyte after long time experiments did not reveal Fe, Ni or Cr ions, (see ESI†) confirming that the current measured during the chronopotentiometry very likely does not arise from oxidation or dissolution. However to further exclude also "inner oxidation" (oxidation of the metal matrix below the oxide layer) during operating it is indispensable to quantify the real oxygen evolution efficiency. We determined the Faradaic efficiency of sample Elox300 (Fig. S3, ESI†). Fig. 1c shows the curve course of the dissolved oxygen in 0.1 M KOH during chronopotentiometry conducted at 10 mA cm^{-2} with the time (black curve) in comparison with the theoretically possible increase of dissolved oxygen on the basis of 100% charge to oxygen conversion (100% Faradaic efficiency; red line). The course of both curves shows a good agreement and the Faradaic efficiency of the OER of sample Elox300 in 0.1 M KOH at 10 mA cm^{-2} and at 260 mV overpotential was found to be 75.5% after 4000 s running time. A significant higher Faradaic efficiency (95.7%) close to the theoretical possible value of 100% could be achieved after 60 000 s of chronopotentiometry at 1 mA cm^{-2} current density, respectively at 215 mV overpotential (see Table S2, ESI†) proving the very good electrocatalytic oxygen evolution properties. A significant deviation of both curves over time (Fig. 1c), was also obtained by other groups[33] and is as such not unusual as is a decreasing Faradaic efficiency at higher current densities. Particularly the latter might up to some extent be ascribed to a slight measurement inaccuracy of the method chosen: We started the experiment at almost 0 mg O$_2$ per l and went within chronopotentiometry toward saturation. We assume that at relative high potentials apparently undissolved oxygen gas bubbles are generated, *i.e.* oxygen cannot be dissolved with the speed with which it is formed. However, a significant decrease of Faradaic efficiency by increasing current densities (from 97% at 1 mA cm^{-2} to 43% at 10 mA cm^{-2}) was also obtained by Qiu *et al.*[21] for Ni–Fe containing nanoparticles in 1 M KOH.[21]

2686 | *Energy Environ. Sci.*, 2015, **8**, 2685–2697

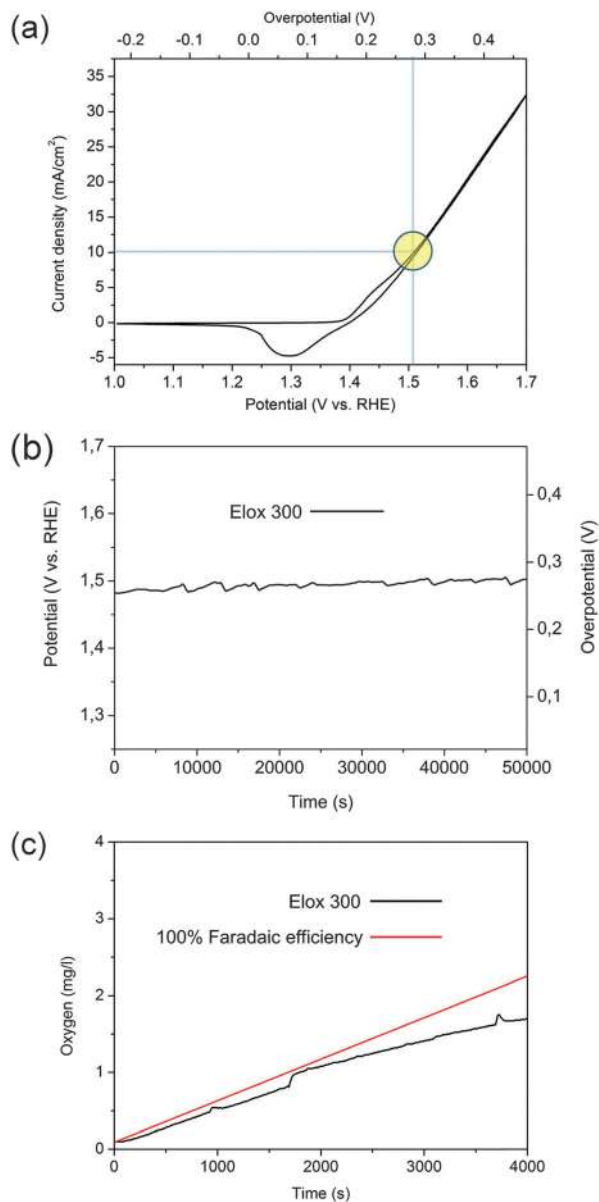This journal is © The Royal Society of Chemistry 2015

Fig. 1 Electrocatalytic oxygen evolution properties of surface oxidized AISI 304 in alkaline medium. (a) Cyclic voltammogram of sample Elox300 recorded in 0.1 M KOH after chronopotentiometry for 50 000 s performed in 0.1 M KOH at 10 mA cm^{-2}. No IR compensation was performed. Scan rate: 20 mV s^{-1}; step size: 2 mV. The electrode area was 1.5 cm^2. (b) Long-term chropotentiometry plot of sample Elox300 performed at 10 mA cm^{-2} in 0.1 M KOH. The electrode area was 1.5 cm^2. The average overpotential amounted to 269.2 mV at 10 mA cm^{-2}, the start potential (t = 90 s) was 1.482 V vs. RHE, the end potential (t = 50 000 s) was 1.503 V vs. RHE corresponding to 254 mV overpotential (t = 90 s), respectively 275 mV overpotential (t = 50 000 s). (c) Correlation of oxygen evolution of sample Elox300 in 0.1 M KOH (black curve) determined with an optical dissolved oxygen (OD) sensor using the so-called fluorescence quenching method with the charge passed through the electrode system (red line corresponds to 100% Faradaic efficiency). Current density: 10 mA cm^{-2}; average overpotential within the 4000 s plot: 260 mV. The electrode area was 1.5 cm^2. Amount of the electrolyte: 2.3 l; start value of dissolved oxygen: 0.09 mg l^{-1} (t = 0 s); end value of dissolved oxygen (t = 4000 s): 1.33 mg l^{-1}. Faradaic efficiency of the OER after 4000 s runtime: 75.5%.

In terms of catalytic activity sample Elox300 is on the level of the samples with the highest ever measured activity values:[34–41] NiCo$_2$O$_4$–graphene hybrid;[39] Ni$_3$S$_2$ nano array supported by Ni metal;[40] CuFe(MoO$_4$)$_3$;[41] Pr$_{0.5}$Ba$_{0.5}$CoO$_3$;[38] NiCo$_2$O$_4$ aerogel;[42] Ni$_x$Fe$_y$(OH)$_2$[22] and Ni$_x$Fe$_y$O$_z$ nanoparticles supported on glassy carbon.[21] On this account the view that these synthesized oxides, sulfides or hydroxides show superior electrocatalytic OER characteristics in alkaline media when compared to metal surfaces oxidized via straightforward approaches can be refuted.

It turned out that neither an extension of the anodization time from 300 to 480 min realized in case of sample Elox480, nor a cyclic switching between different potentials (cyclic oxidation, sample EloxCycl) could further improve the catalytic properties (Table 1 and Fig. S4–S6, ESI†). In case of sample Elox480 a overpotential of 292 mV at 10 mA cm^{-2} could be derived from steady state measurements and the overpotential of EloxCycl amounted to 395 mV at 10 mA cm^{-2} both of which determined in 0.1 M KOH (Table 1 and Fig. S5, ESI†).

We compared samples Elox300 and Elox480 with IrO$_2$–RuO$_2$ coated titanium (sample IrO$_2$–RuO$_2$, Fig. S7, ESI†) which can be considered as an established water splitting catalyst[4–12] in terms of electro catalytic activity (Fig. 2a and b). Differences with respect to the OER currents of all three samples at different voltages respectively overpotentials can be extracted from the Tafel plots shown in Fig. 2b. Superior electrocatalytic behaviour was found for both of our samples when compared with IrO$_2$–RuO$_2$ which showed an overpotential of 452 mV derived from 40 000 s of chronopotentiometry at 10 mA cm^{-2} in 0.1 M KOH (Fig. 2a). Sample Elox300 and Elox480 achieved in 0.1 M KOH the same current density at 269.2 mV overpotential (Fig. 1b) and at 292 mV (Fig. S5, ESI†) respectively which corresponds to ∼140 mV difference between our samples and IrO$_2$–RuO$_2$. This voltage difference between the oxidized steel samples and IrO$_2$–RuO$_2$ increases with increasing current density from around 50 mV at 0.66 mA cm^{-2} till 200 mV at 20 mA cm^{-2}, i.e. especially in the high potential region IrO$_2$–RuO$_2$ loses significantly performance which is displayed by the rising Tafel slope (Fig. 2b). The gap within the OER performance was particularly huge when sample Elox300 was compared with untreated AISI 304 steel (Fig. 3a–c). The most obvious differences between surface oxidized AISI 304 steel and untreated AISI 304 steel emerged from electrochemical measurements shall be listed briefly:

1. The corresponding voltage/current curve of sample Elox300 (Fig. 3b) was found to be stiffer than the CV curve of AISI304 (Fig. 3a; see also Fig. 5b). Samples Elox300 (AISI304) reached 1, 5 and 10 mA cm^{-2} current density at potentials of 1.402 (1.569), 1.447 (1.63) and 1.504 (1.68) V vs. RHE which corresponds to 174 (342), 219 (402) and 276 (452) mV overpotential respectively (Fig. 3a and b). In addition, the potential at which the current starts to significantly increase undergoes a negative shift (140 mV) from 1.52 V vs. RHE (AISI304) to 1.38 V vs. RHE (Elox300) (Fig. 3a, b and 5b). 2. Different outcome from steady state measurements: a substantial horizontal shift of the Tafel line assigned to sample Elox300 compared to the corresponding Tafel line of AISI304 toward lower potentials (Fig. 3c) also proves the
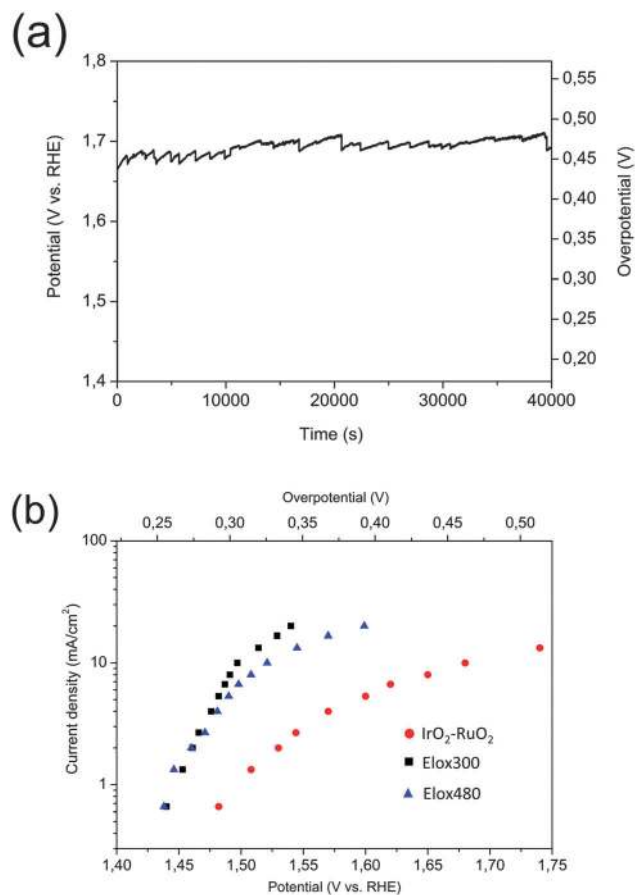
This journal is © The Royal Society of Chemistry 2015

Energy Environ. Sci., 2015, **8**, 2685–2697 | **2687**

Fig. 2 A comparison of the electrocatalytic oxygen evolution properties of the surface oxidized samples Elox300 and Elox480 with purchased IrO_2–RuO_2 determined in alkaline solution. (a) Long-term chropotentiometry plot of sample IrO_2–RuO_2 performed at 10 mA cm^{-2} in 0.1 M KOH. No IR compensation was performed. The electrode area was 2 cm^2. The average overpotential amounted to 452 mV at 10 mA cm^{-2}, the start potential (t = 90 s) was 1.668 V vs. RHE, the end potential (t = 40 000 s) was 1.688 V vs. RHE corresponding to 439 mV overpotential (t = 90 s), respectively 460 mV overpotential (t = 40 000 s). (b) Tafel plots of samples Elox300, Elox480 and IrO_2–RuO_2. Average voltage values for the Tafel plots were derived from 200 second chronopotentiometry scans at the corresponding current densities. IR compensation was performed for all plots taking into account the values for electrolyte resistance from Table 3. The electrode area is 1.5 cm^2 (Elox300, Elox480), respectively 2 cm^2 (IrO_2–RuO_2).

meaningful enhancement of the electrocatalytic properties upon the applied surface oxidation. Dual Tafel regions can be allocated to both samples with lower slopes at lower overpotential regions (Elox300: 49 mV dec^{-1} $\cong$ 2.303 × 5RT/6F; AISI304: 66 mV dec^{-1}) and higher slopes at higher overpotential regions (Elox300: 150 mV dec^{-1}, AISI304: 250 mV dec^{-1}). This implies either a different OER mechanism on the surfaces of samples AISI304 and Elox300 or a different rate determining step. The Tafel slope of Elox300 in diluted KOH in lower overpotential region (2.303 × 5RT/6F) agrees very well with earlier reported Tafel slopes for NiFe alloy,[43] iron electrodes,[12] carbon supported NiO nanoparticles[21] or for "fresh" Ni metal surfaces[12] whereas earlier papers reported on slopes up to 80 mV dec^{-1} in lower potential region in case of fresh nickel-oxide electrodes.[45]

3. The abrupt current increment within CVs (Fig. 3b) in case of oxidized steel was accompanied by the visible release of gas. In sharp contrast to the corresponding experiments with surface oxidized samples (Fig. 1a–c) polarization currents caused by untreated steel (Fig. 3a and c) were at the very beginning of the measurements not accompanied by the formation of gas bubbles. Therefore currents, determined for sample AISI304 via steady state (Fig. 3c) or non-steady state (Fig. 3a) techniques, arise, according to our conviction, to a large share from the oxidation of the bare steel surface. 4. In contrast to the CV of AISI304 sample (Fig. 3a) the CVs of the electro-oxidized samples Elox300 and Elox480 (Fig. 3b and Fig. S6, ESI†) showed a pronounced cathodic voltammetric sweep at potential 1.2–1.42 V. vs. RHE typically obtained by CVs of Ni containing samples[21,22,28] and which we clearly attribute to the Ni(III)–Ni(II) reduction taking into account the drastic oxidation of the steel at last evoking the expectation that the oxidation state of Ni on the surface is throughout +3. From OER on pure Ni electrodes is known that there exists a direct proportionality between the amount of active material based on the Ni(II)/Ni(III) redox system and the charge capacity, Q, calculated by integrating this cathodic voltammetric sweep between the uppermost limit and ca. 1 V vs. RHE.[44,45] The integrated Q therefore allows prediction of the overall OER performance. Such an analysis performed between ∼1.4 V vs. RHE and 1 V vs. RHE delivers Q = 27.57 mC cm^{-2} (Elox300; Fig. 3d) respectively 22.55 mC cm^{-2} (Elox480; Fig. S8, ESI†) determined in 0.1 M KOH at 20 mV s^{-1} sweep rate which impressively implies a high amount of electrocatalytic active material. Significant lower charge capacities and, deriving there from a lower amount of OER active material was obtained for the sample EloxCycl (1.20 mC cm^{-2}, Fig. S9, ESI†), AISI304 (0 mC cm^{-2}) respectively by Lyons et al. (<8 mC cm^{-2}) for freshly polished Ni electrodes, the latter calculated within a voltage region of 0 and 0.675 V vs. Hg/HgO; determined at 40 mV s^{-1} sweep rate in 1 M NaOH.[12] Thus the integrated Q of the oxidized AISI 304 samples Elox300 (27.57 mC cm^{-2}), Elox480 (22.55 mC cm^{-2}) and EloxCycl (1.2 mC cm^{-2}) are in line with the determined OER performance in 0.1 M KOH of the samples Elox300 (269.2 mV overpotential), Elox480 (292 mV overpotential), Elox-Cycl (347 mV overpotential) respectively (see Table 1). Studies dealing with Ni, Fe based electrocatalysts also reported on a significant integrated charge for the oxidation wave.[19] Fig. 1a and 3b show that there is indeed a substantially less pronounced oxidation peak at around 1.45 V versus RHE in the CV of sample Elox300.

This negligible oxidation wave could have been caused by surface Ni^{2+} ions although from Ni–Fe based OER electrocatalysts it is known that cathodic and anodic wave are usually somewhat more separated.[21] Therefore we would have expected the anodic wave earlier, i.e. at potentials around 1.375 V versus RHE. However if we assume that this anodic sweep results from Ni(II)–Ni(III) oxidation we can integrate the total charge under this Ni^{2+} oxidation wave Q and then estimate the influence of surface Ni^{2+} ions on the total active mass based on the Ni(II)/Ni(III) redox system.[19] In doing so the integrated Q amounts to 0.03 and is therefore negligible (0.03 mC cm^{-2}) in comparison with the corresponding

2688 | Energy Environ. Sci., 2015, 8, 2685–2697
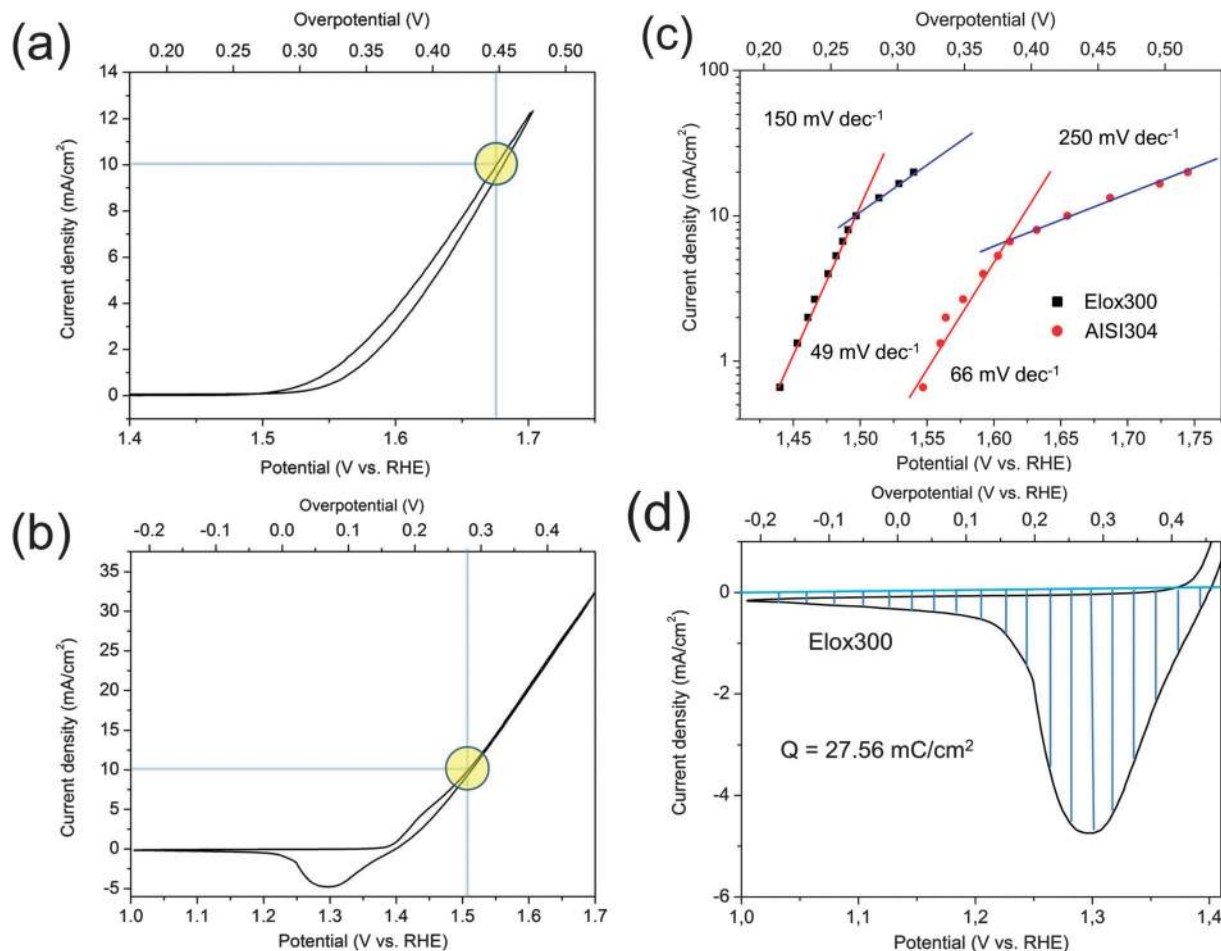
This journal is © The Royal Society of Chemistry 2015

Fig. 3 A comparison of the oxygen evolution properties of untreated AISI 304 steel with sample Elox300 determined in 0.1 M KOH. No IR compensation was performed for steady state and non-steady state measurements (a) Cyclic voltammogram of untreated AISI 304 recorded in 0.1 M KOH at 10 mA cm^{-2}. Scan rate: 20 mV s^{-1}; step size: 2 mV. (b) Cyclic voltammogram of sample Elox300 recorded in 0.1 M KOH after chronopotentiometry for 50 000 s performed in 0.1 M KOH at 10 mA cm^{-2}. Scan rate: 20 mV s^{-1}; step size: 2 mV. (c) Tafel plots of untreated AISI304 steel and sample Elox300. Average voltage values for the Tafel plots were derived from 200 seconds of chronopotentiometry scans at the corresponding current densities. IR compensation was performed for all plots taking into account the values for electrolyte resistance from Table 3. The electrode area was 1.5 cm^2 (Elox300), respectively 2 cm^2 (AISI304). (d) Cyclic voltammogram (current density vs. overpotential scan) of sample Elox300 measured in 0.1 M KOH. Determination of the charge capacity Q was by integrating the cathodic voltammetric sweep between 1.7 V vs. RHE and 1 V vs. RHE. Q amounted to 27.57 mC cm^{-2}. Scan rate: 20 mV s^{-1}; step size: 2 mV.

value assigned to the cathodic sweep (27.57 mC cm^{-2}; see Fig. 3d manuscript).

CV curves not only allow to predict the amount of catalytic active Ni species but also the Ni:Fe stoichiometry. In simple terms: CV curves of binary (pure) Ni–Fe systems show a cathodic, as well as an anodic sweep if the Ni content ≥69 atom%. Just a cathodic sweep can be obtained if the Ni content is between 20 and 69 atom% and finally neither an anodic-nor a cathodic sweep can be obtained if the material contents less than 20 atom% Ni.[20–22] Louie and Bell,[20] Trotochaud and Boettcher et al.[22] as well as Li et al.[21] reported on the generation and investigation of electro-deposited Ni–Fe oxide–hydroxide thin films and the generation of Ni–Fe nanoparticles, respectively. They obtained optimal electrocatalytic performance (280 mV overpotential at 10 mA cm^{-2} in 0.1 M KOH) for Ni contents of 59 atom% (just a cathodic sweep)[20] and 69% (cathodic plus anodic sweep),[21] as well as 250 mV overpotential

at 1 mA cm^{-2} in 0.1 M KOH for Ni contents of 75% (cathodic plus anodic sweep).[22]

XPS spectroscopic investigations

XPS spectroscopy was used to provide an answer to the crucial question, whether a full comparability is guaranteed between our samples and the before mentioned nano scaled Ni, Fe based samples.[20–22] In particular we were interested to examine whether in addition to the absolute comparable electrochemical properties (OER performance, CV curve) the composition of these particles or films are comparable. Indeed performed XPS experiments supported this expectation. The XPS experiments confirmed that in comparison with untreated steel (Table 2 and Fig. 4a) a significant higher Ni content could be detected on the surface of the electro-oxidized samples. For Elox300 the Ni content on the surface reached 67%, representing a 17 fold increase (AISI304: 4% Ni, 16.3% Cr, 79.7% Fe; Table 2), and

This journal is © The Royal Society of Chemistry 2015

Energy Environ. Sci., 2015, 8, 2685–2697 | 2689

Table 2 Cationic distribution and position of the $2p_{3/2}$ main lines of Cr, Fe, and Ni of samples Elox300, Elox480, EloxCycl and a steel reference sample (non-treated AISI 304 steel) derived from the XPS measurements presented in Fig. 4. Measurements performed before and after carrying out the chronopotentiometry scans (0.1 M KOH; 10 mA cm^{-2} current density; duration: 50 000 s) showed the same value

Element	Cationic distribution (at%)			Position of $2p_{3/2}$ line (± 0.25 eV)		
	Cr	Fe	Ni	Cr	Fe	Ni
Sensitivity factor	2.488	1.964	2.309			
Elox300	0%	33.0%	67.0%	576.5 eV	711.75 eV	856.0 eV
Elox480	0%	36.8%	63.2%			
EloxCycl	5.6%	73.4%	21.0%			
Reference	16.3%	79.7%	4.0%	576.5 eV	(706.5 eV)	(852.5 eV)
					710.1 eV	855.75 eV

therefore exceeds the level of the iron content (33%). Ni was, as expected, shifted to the surface, while Cr could be suppressed leading to a thin film consisting of pure Ni, Fe oxide (Table 2 and Scheme 1).

This tendency was obtained with respect to all electro-activated samples, although the Ni enrichment on the surface was less pronounced for samples Elox480 (62.2%) and EloxCycl (21%; Table 2 and Fig. 4a). Further significant differences between samples Elox300/Elox480 and AISI304 exposed by XPS experiments: in the Fe 2p spectra we find a small metallic fraction for the steel reference sample (Fig. 4b). Besides iron the reference steel sample also contains fractions of metallic Ni (Fig. 4a). Both findings support the assumption that in terms of sample AISI304, polarization currents arise from oxidation of the catalyst itself and not from OER. Unoxidized Fe, Ni species could not be determined on the surface of the oxidized samples Elox300, Elox480 and EloxCycl (Fig. 4a and b). This again emphasizes, that the current determined by chronopotentiometry for the surface oxidized samples arises from OER.

Most likely is that Ni is present in form of γ-NiOOH[46,47] on the surface (Fig. 4a). We found no direct hints proving the existence of significant amounts of Ni(II) compounds on the surface, which coincides with the absence of a significant oxidation peak within the potential region 1–1.7 V vs. RHE (originated from Ni(II)–Ni(III) oxidation[48]) in the CV curves of sample Elox300 (Fig. 1a).

The absence of Ni(II) on the surface of our surface oxidized steel samples can be explained best by the harsh oxidative conditions during electro activation creating extreme anodic potentials. We initially did not expect the existence of Ni(II) species on the periphery/surface of the activated steel. For the Fe $2p_{3/2}$ binding energies the FeOOH species of iron clearly dominate on the surface of sample Elox300 compared to the peak positions found for the reference compounds[46,49,50] (Fig. 4b). Most likely, the Cr is present in form of Cr^{III} either as Cr$_2$O$_3$ or Cr(III) hydroxide or as a mixture of both forms (Fig. 4c).

The principle result of the XPS experiments using our electro-activated AISI 304 steel samples is that anodization under harsh conditions leads (i) to an ultra-thin layer consisting of a Fe–Ni oxide system with a purity >99%. (ii) The optimal electrochemical properties were found to be 67% Ni and 33.0%
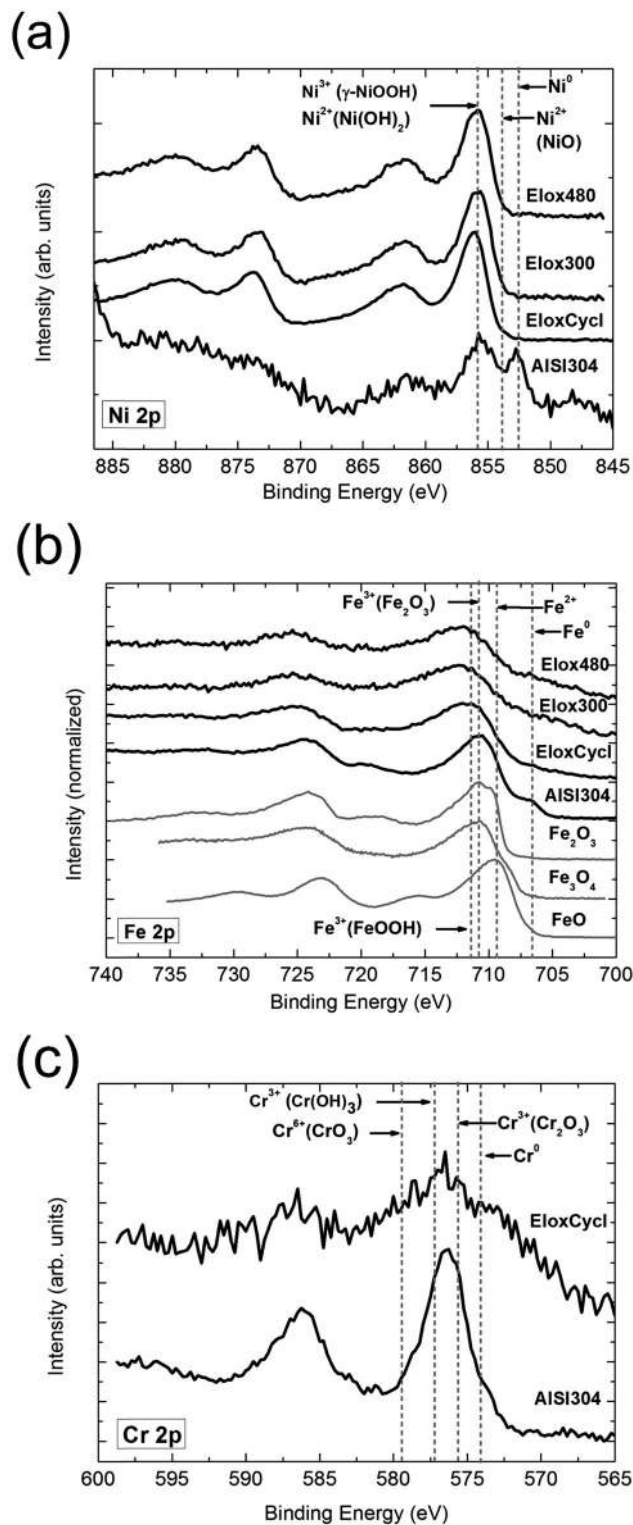

Fig. 4 XPS results of the samples Elox300, Elox480, EloxCycl and Ref (untreated AISI 304 steel). (a) Ni 2p core levels. Vertical lines indicate binding energies of metallic Ni, as well as γ-NiOOH, Ni(OH)$_2$ and NiO reference compounds as a guide to the eyes.[46,47,69] (b) Fe 2p core levels. Binding energies for FeO, Fe$_2$O$_3$ and Fe$_3$O$_4$ used as reference compounds are indicated by vertical lines.[49] (c) Cr 2p core levels. Binding energies of metallic Cr as well as CrO$_3$, Cr(OH)$_3$ and Cr$_2$O$_3$ reference compounds are also indicated by vertical lines as a guide to the eyes.[46]
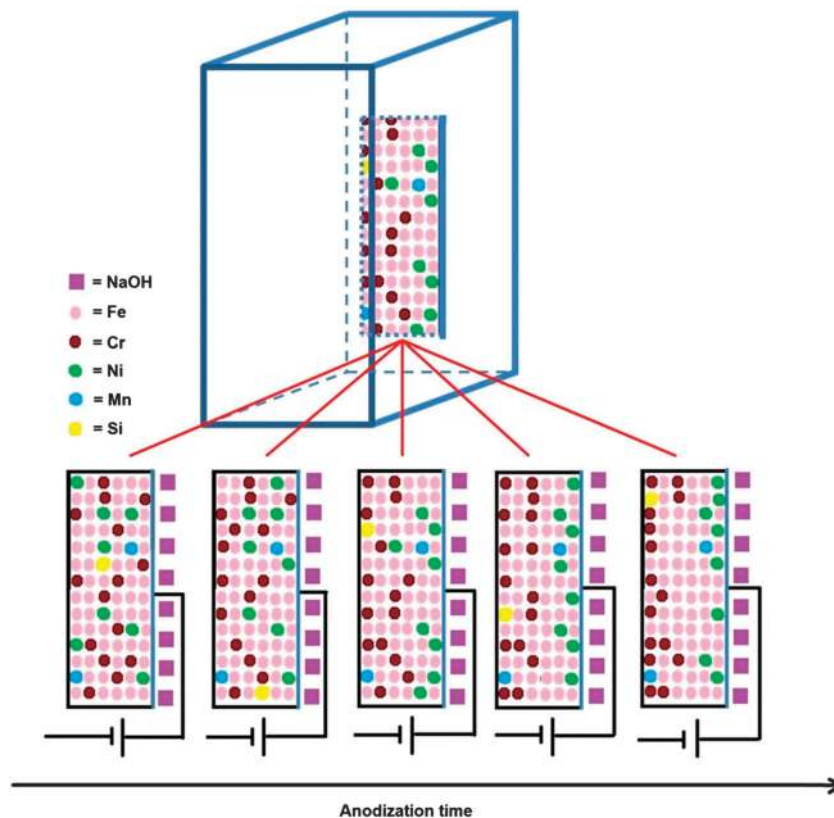
Scheme 1 Two dimensional presentation of the enrichment of nickel on the surface of electro-anodized AISI 304 steel under harsh conditions. The scheme shows a simplified representation of the 3 dimensional layer forming process *via* face cutouts "recorded" after different anodization times.

Fe as shown in Table 2. In relation to the surface composition (Table 2 and Fig. 4) and in relation to the electrocatalytical properties (Fig. 1a and Fig. S6, ESI†) samples Elox300 and Elox 480 line up perfectly with the before mentioned Ni–Fe based nanoscaled compounds introduced by Louie and Bell,[20] Trotochaud and Boettcher *et al.*[22] as well as by Li *et al.*[21]

All three groups independently developed a material with comparable composition and similar OER performance. It is well known that size reduction[51] down to nm regime goes along with changes within manifold properties[52,53] above all with an increment of the surface to volume ratio and the striking question arising from this is whether nanoparticles that basically consists of 69% Ni and 31% Fe[21] can be compared with a piece of oxidized solid metal with 14 g weight which periphery composes of 67% Ni and 33% Fe (sample Elox300). Also important is to understand whether an increase of the catalytic active surface area during surface oxidation of AISI 304 steel could be the origin for the drastic increase of OER performance.

The origin of the superior OER activity-varying the Ni : Fe ratio. To clarifying whether the OER properties of a macroscopic Ni–Fe based electrocatalyst is substantially determined by the Ni : Fe ratio we checked the electrocatalytic OER properties of alloys basically consisting of Fe and Ni that strongly differ in their Ni:Fe stoichiometry. We performed chronopotentiometry measurements for 2000 s in 0.1 M KOH and determined the potential *vs.* RHE required to deliver 10 mA cm^{-2} current density.

In addition to our samples Elox300 (67% Ni), Elox480 (63.2% Ni) and EloxCycl (21% Ni), Ni42 (Fig. S10, ESI†), an alloy with 42% Ni as well as Iron with 0% Ni has been included in the sample series.

The results are shown in Fig. 5a and confirm differences of the electrocatalytic OER properties – we for example see a decrease in overpotential with increasing Ni content. Ni42 (42% Ni) with an overpotential of 347 mV and iron (0% Ni) with 510 mV overpotential line up perfectly with our surface oxidized samples Elox300 (67% Ni; 269.2 mV), Elox480 (63.2% Ni; 292 mV) and EloxCycl (21% Ni; 395 mV).

Influence of the surface oxidation procedure on the catalytic active surface area

Typically the surface oxidation treatment leads to significant horizontal shifts of the corresponding CV curves in comparison with the CV curve of untreated steel towards lower voltage, respectively to lower overpotential as demonstrated on sample Elox300 in Fig. 5b. This horizontal shift of the CV curve by 140 mV can in our opinion only be explained by a drastic change of the chemical nature of the surface resulting from the performed surface activation procedure as stated above in the XPS spectroscopy experiment.

An increase of the active area during the electro-oxidation procedure could in principle also be the reason for higher currents at defined potential after surface modification *via*
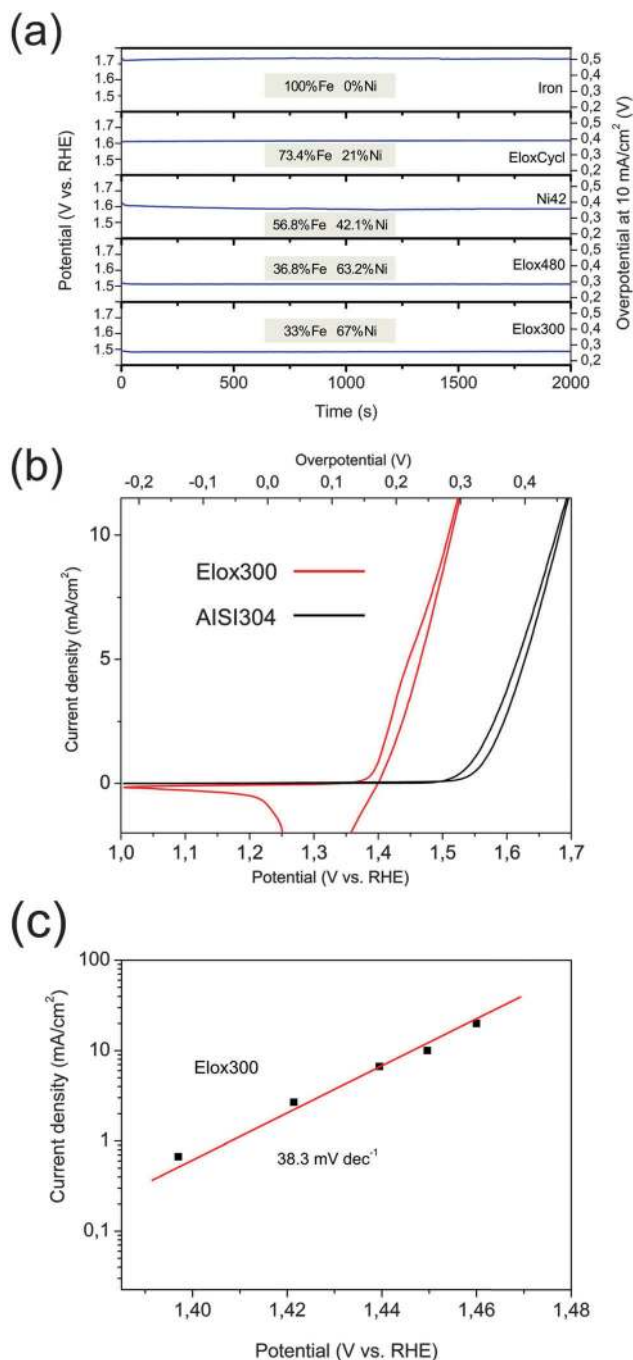
This journal is © The Royal Society of Chemistry 2015

Energy Environ. Sci., 2015, **8**, 2685–2697 | **2691**

Fig. 5 (a) The dependence of the electrocatalytic oxygen evolution properties of iron–nickel based materials of the Ni : Fe relation on the periphery. Chronopotentiometry plots of samples EloxCycl, Elox300 and Elox480 in comparison with pure iron (iron) and AISI Ni42 (Ni42) determined in 0.1 M KOH at 10 mA cm^{-2}. No IR compensation was performed. Average overpotential at 10 mA cm^{-2}: 510 mV (iron), 395 mV (EloxCycl), 347 mV (Ni42), 292 mV (Elox480) and 269.2 mV (Elox300). (b) A comparison of cyclic voltammograms of sample Elox300 and AISI304. The negative horizontal shift between both CV curves amounted to $\sim$140 mV. (c) Tafel plot of sample Elox300 in 5 M KOH. Average voltage values for the Tafel plots were derived from 200 second chronopotentiometry scans at the corresponding current densities. Electrode geometry: 1 mm distance between CE and WE; the electrode area was 1.5 cm^2.

anodization, but this would lead to a vertical shift of the CV curve in the direction of higher current intensities. To further examine and exclude a potential increase of the active area as the basis for the observed results we undertook additional STM and AFM experiments:

As seen in the STM and AFM images of sample AISI304 (Fig. S11 and S12, ESI†) and sample Elox300 the surface of the anodized sample Elox300 (Fig. S13 and S14, ESI†) is rather smoother than the surface of the untreated sample (Fig. S11 and S12, ESI†).

Prior to the anodization the untreated steel and the bare metal of the samples were grinded with sanding paper grit-600 prior to the AFM and STM experiments. The furrows and grooves caused by the sanding paper can still be seen on the corresponding AFM images (Fig. S11, ESI†), whereas on the surface of the anodized sample Elox300 the traces of mechanical machining cannot be obtained anymore, and the surface appears smooth (Fig. S13 and S14, ESI†). These findings are inconsistent with an increase of the catalytic active area.

The catalytic active species

Despite the recent renewal in interest in OER at metal oxide based nano- and macrocrystalline electrocatalysts, some of the discussed active species are still disputed.[12] However high resolution XPS spectra of our samples Elox300 and Elox480 (Fig. 4a) suggested γ-NiO(OH) as a potential catalytic active OER species or at least as the dominating source for the OER active species on the oxidized steel surface in alkaline regime. To achieve substantial support for this theory it makes sense to evaluate current knowledge of catalytic active OER species on pure Ni metal electrodes. According to Bode et al. two coexisting limiting discharged phases, α-Ni(OH)$_2$ and β-Ni(OH)$_2$, and two limiting charged phases, γ-Ni(III/IV) and β-NiOOH play a major role within the electrocatalytic evolution of oxygen on Ni metal surfaces.[54] Strong oxidative conditions automatically rule out Ni in oxidation state +2, i.e. the phases α-Ni(OH)$_2$ and β-Ni(OH)$_2$. In addition it is known that β-NiOOH can be converted to the gamma phase by so-called overcharge at extreme anodic potentials,[12] suggesting that indeed γ-NiOOH constitutes the catalytically active centre on pure Ni under harsh oxidative conditions in an alkaline medium. This interpretation is also consistent with the outcome of polarization experiments performed with Ni metal done by Lyons et al.,[12] and with the recent density functional theory calculations (DFT) by Rossmeisl et al.[55,56] the latter described the formation of a superoxy (OOH) species as a consequence of an addition of OH$^-$ on top of O atom coordinated by the metal surface as the rate determining step (RDS). Based on this analysis a dissociation of OH$^-$ ions to form adsorbed O atoms on Ni surfaces takes place at potentials at which OER occurs. At a certain point the coverage of the Ni surface with O atoms is large enough to make direct OH$^-$ addition under formation of NiOOH fragments more favourable relative to direct coordination of OH$^-$ ions to Ni cations.
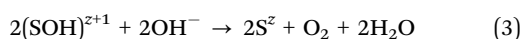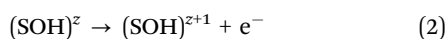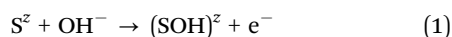
The role Fe plays in enhancing the Ni-based oxygen evolution reaction electrocatalysts is up to now not fully understood. Singh et al. reported on interactions between low d-electron

2692 | Energy Environ. Sci., 2015, 8, 2685–2697

This journal is © The Royal Society of Chemistry 2015

structured atoms and ions (Cr) with high d-electron species like Co, Ni or Fe typically occurring in spinel-type catalysts which enhances the electrocatalytic properties, an effect that is called hypo-hyper d interbonding effect.[57–60] As a short distance phenomenon it can only occur between ions within close neighbour sphere. We therefore conclude that due to these or similar short distance interactions during the electro activation process a perfect arrangement of Ni ions at atomic scale is fulfilled which therefore is responsible for the very good catalytic properties. For electro deposited Ni/Fe oxyhydroxide thin films the effects caused by Fe incorporation were discussed in detail by Boettcher et al.[22] In a parallel report we describe the surface modification of AISI 304 steel inter alia via chlorine gas which caused a Cr enriched surface, i.e. a suppression of Ni and a Cr enrichment was found.[61] However this treatment resulted in a substantial weaker enhancement of the electro-catalytic properties.

The mechanism of the OER on the surface of the oxidized steel samples

Mechanistic information of the OER can only be extracted from steady state kinetic data up to the RDS. Possible mechanism of the formation of molecular oxygen starting from surface bonded Ni-superoxy species, such as the subsequent steps after RDS are still controversial discussed, speculative and not based on the isolation and identification of intermediate species.[12] We propose to assume a reaction pathway (eqn (1)–(3)) that is linked with OER on non-noble metal surfaces introduced by Yeager et al.[62] in which S is the mentioned active site of the catalyst (γ-NiOOH):

$$S^z + OH^- \rightarrow (SOH)^z + e^- \tag{1}$$

$$(SOH)^z \rightarrow (SOH)^{z+1} + e^- \tag{2}$$

$$2(SOH)^{z+1} + 2OH^- \rightarrow 2S^z + O_2 + 2H_2O \tag{3}$$

However we could not extract the reaction order from experimental data. For sample Elox300 a Tafel slope of 49 mV dec^{-1} could be obtained in 0.1 M KOH solution (Fig. 3c). From literature it is known that Tafel slopes significantly higher than $2.303 \times 2RT/3F$ (39.4 mV dec^{-1} at 25 °C) are difficult to be rationalized by a simple electrode/solution interface model.[12] Approaches based on more complicate, i.e. dual barrier models can help to extract reasonable reaction orders from $(\partial \log i/\partial \log a)_E$ behaviour where i is the current density at a defined potential E and a is the activity. Meyer[63] found that under dual barrier conditions the reaction order m_s depends on $(\partial \log i/\partial \log a)_E$ behaviour according to:

$$\left(\frac{\partial \log j}{\partial \log a}\right)_E = \frac{m_s \beta_f}{\beta_f + \beta_s}$$

Here β_f is the electron transfer symmetry factor for field assisted charge transport through the oxide and β_t is a composite symmetry factor taking account the two potential energy barriers.

However, one and the same sample needs to show identical Tafel slopes at different KOH concentrations a basic prerequisite

that has to be fulfilled in order to extract a meaningful reaction order from $(\partial \log i/\partial \log a)_E$ behaviour.

Depending on the KOH concentration, Tafel slopes in the range 38.3 mV–49 mV dec^{-1} (Fig. 3c and 5c) were determined for the same sample (ELOX300) at KOH molarity 0.5 to 5. The lowest Tafel slope was determined in 5 M KOH (38.3 mV dec^{-1}, Fig. 5c). Different slopes at different concentrations can be rationalized by different OER mechanism but could also be indicative of changes in intermediate coverage, respectively of changes in the rate determining step while moving from lower (0.1 M) to higher (0.5, 1, 2, 5 M) KOH concentrations. Burke and Twomey discussed the effects of increasing alkalinity on potentially catalytic active species during polarization in NaOH solutions.[44] However a reliable reaction order for the OER reaction on the surface of our oxidized steel samples cannot be extracted from the Tafel behaviour by determination of $\log i/\log a_{OH^-}$ at constant potential.

The mechanism of the Ni enrichment on the surface of the oxidized steel samples

The enrichment of nickel on the surface of the electro-modified alloy can in principle be explained by a dissolution process, a dissolution–precipitation mechanism and by electromigration[64,65] of some of the alloy components. Besides coloration of the electrolyte and precipitation deposited on the CE we also determined a significant reduction in weight of the steel specimen during the surface treatment performed in strong alkaline regime. These are hints that dissolving of at least some of the ingredients of the steel in the sodium hydroxide electrolyte takes place.

In order to prove whether dissolving of Cr and Fe out of the metal frame is indeed the origin of the Ni enrichment on the surface of our electro-activated samples the electrolyte (7.2 M NaOH) and also the material deposited on the CE after 300- respectively 480 min of anodization were analyzed utilizing atomic emission spectroscopy (AAS; see Experimental part, Table S3; ESI†). In total five anodization experiments, three of them after 300 min of anodization, and two of them after anodization for 480 min were investigated (Table S3, ESI†).

The mass loss of the steel specimen amounted to 6.15 and 17.15 mg (Table S3, ESI†), depending on the duration of the procedure.

The composition of the electrolyte

In procedures utilized we detected an amount of chromium in the electrolyte that exceeded the sum of the amounts of Fe and Ni in the electrolyte significantly (Table S3, ESI†) thus suggesting a depletion of Cr on the surface of AISI 304 steel during electro activation. This interpretation agrees with the changes within the composition of the surface of the samples during electro activation: XPS experiments showed (Table 2) no Cr on the surface of samples Elox300 and Elox480 whereas the surface of untreated steel consisted of 16.3% Cr (Table 2). The higher solubility of the Cr-oxide species formed on the surface of the steel during electro activation in strong alkaline medium in comparison with the corresponding solubility of Fe- and Ni-oxide species seems

to be a reasonable explanation for the high Cr content in the electrolyte. However, differences within the solubility's of the bare metals Fe, Cr and Ni in the NaOH electrolyte should play a minor role given that our electro activation is accompanied by OER, which cannot occur on the metal surface, but does on the oxidized surface.

The composition of the precipitate formed on the CE

In all activation procedures studied the precipitation formed on the CE mainly represents iron besides small amounts of nickel. Ni- and Fe-oxide species formed in solution during electro-activation can (unlike Cr-oxide) be reduced cathodically and therefore precipitate on the CE. This finding is not astonishing, as other studies such as Zou *et al.* reported on the electrodeposition of Fe films from Fe_2O_3 in strong alkaline solutions,[66] and a number of groups[67,68] confirmed the electrodeposition of Ni or Ni containing alloys from aqueous solutions. In addition Fe, Ni are insoluble in strong alkaline medium (crucibles are made of Ni) which explains why Fe, Ni containing layers formed on the CE during anodization do not dissolve in NaOH.

Thus the overall conclusion from the AAS study that the electrolyte basically contents Cr and the precipitation formed on the CE basically contents Fe supports the assumption that Ni enrichment on the surface of stainless steel AISI 304 during electro-activation occurs from dissolution of Cr and Fe from the steel surface, whereas Ni by and large remains in the framework. The total Ni detected using AAS spectroscopy (in electrolyte solution plus precipitation on CE) after carrying out the anodization according to Elox fix 480 (2), Elox fix 300 (2), Elox fix 300 (3) is indeed below the Ni content on the surface of the untreated stainless steel, *i.e.* <4%, as shown by XPS spectroscopy (Table 2). This confirms our theory of enrichment of Ni on the surface of the anodized steel due to dissolving of Cr and Fe out of the metal frame during anodization.

As part of a precise quantitative analysis, however, we encountered slight deviations in a small number of performed procedures investigated: in fact for Elox fix 300 (1) and Elox fix 480 (1) the steel significantly lost Ni content during electro activation, and also some of the dissolving of Fe out of the alloy was less pronounced as expected. The sum of the amount of detected Ni, Cr, Fe in the electrolyte plus the sum of the amount of detected Ni, Cr, Fe deposited on the CE was found to be 3.842 mg (Elox fix 300 (1)), 13.0589 mg (Elox fix 480 (1)), respectively (Table S3, ESI†). With respect to Elox 300 (1), 55% of the total amount of 3.842 mg detected consists of Fe. The corresponding proportion of Fe in the detected amount of 13.0589 mg for Elox fix 480 (1) was 64% (Table S3, ESI†). The cationic distribution in the outer sphere of untreated stainless steel was found to be 16.3% Cr, 79.7% Fe, 4.0% Ni. Since the AAS experiment mentioned before resulted in iron contents of 55% and 64% in the total amount detected, we did expect Fe enrichment on the surface of the electro-activated steel samples, and not an iron depletion as obtained by XPS spectroscopy (Table 2; Elox300: 33% Fe; Elox480: 36.8%). Moreover, for both procedures the Ni contents in the detected material gave 0.377 mg which corresponds to 9.8% and 1.415 mg which corresponds to 10.8% (Table S3, ESI†). As such both exceeded slightly the content of Ni (4%) in the outer sphere of untreated

AISI 304 steel as shown by XPS spectroscopic analysis (Table 2, sample AISI304).

Conclusions

In summary, a robust oxygen evolution electrocatalyst consisting of earth-abundant elements ensuring an activity at benchmark level was generated by simple surface oxidation of stainless steel AISI 304. The aim of the study was to increase the catalytic performance of the steel regarding OER by creating a thin Ni, Fe oxide layer, a material which is known for its excellent electrocatalytic OER properties, firmly attached to the steel substrate. We found that when electro-oxidation is performed using AISI 304 metal alloy as an anode under particularly harsh conditions (7.2 M NaOH, current density ~1800 mA cm^{-2}, T = 323 K), chromium is completely suppressed in the surface, and an ultra-thin film consisting of $Ni_{0.67}Fe_{0.33}$-oxide (sample Elox300) with a purity as high as 99% is formed on a steel type which is traditionally known for its resistance to corrosion. This layer, most likely originated from a dissolution based mechanism, ensures OER with Benchmark properties as seen in the strong current–voltage behaviour *e.g.* of sample Elox300 in 0.1 M KOH with 10 mA cm^{-2} current density at 1.497 V *vs.* RHE (269.2 mV overpotential) and demonstrated in long term (50 ks) chronopotentiometry plots. An even lower potential of 1.44 V *vs.* RHE (212 mV overpotential) initiated an average current density of 12 mA cm^{-2} in 1 M KOH.

We found that the oxide layer formed on stainless steel AISI 304 upon our procedure creates a stable outer sphere, and the surface oxidized steel samples proved to be inert against longer operating times (>150 ks) in alkaline medium. Faradaic efficiency measurements performed through chronopotentiometry in alkaline regime revealed a charge to oxygen conversion close to 100% and emphasizes that no "inner oxidation" based on further oxidation of the metal matrix below the oxide layer occurs. The composition of the surface layer and the catalytic performance of the specimen is entirely comparable to those obtained by Louie and Bell,[20] Qui and Li,[21] respectively Trotochaud and Boettcher *et al.*[22] for very recently developed highly active Fe–Ni based oxygen evolution electro-catalysts. We were successful in mimicking not only the composition of highly advanced oxygen-evolution electrocatalysts whilst at the same time achieving excellent electrocatalytic ratings in alkaline regime. Based on XPS investigations γ-NiOOH could be identified as the most likely catalytic active species.

We propose that this type of surface modified stainless steel holds significant promise as high-performance oxygen evolution electrocatalysts in the future given their low cost, excellent electrocatalytic properties (overpotential of 212 mV at 12 mA cm^{-2} current density in 1 M KOH) and ability to be manufactured in large scale dimensions.

Experimental section

Preparation of the samples – electro oxidation of stainless steel (samples Elox300, Elox480) at constant potential

All samples with a total geometry of 100 × 10 × 1.5 mm were constructed from 1.5 mm thick X5CrNi18-10 (304) steel.

Pre-treatment: prior to each surface modification the surface of the metal was cleaned intensively with ethanol and polished with grit 600 SiC sanding paper. Afterwards the surface was rinsed intensively with deionised water. For the electro-oxidation a two electrode set-up was used consisting of the steel sample as WE and a platinum wire electrode (4×5 cm) used as CE. The WE (anode) was immersed 1.3 cm deep (around 3 cm^2 geometric area), and the CE (cathode) was completely immersed into the electrolyte. The electrolyte was prepared as follows: In a 150 mL glass beaker, 25.5 g (0.64 mol) of NaOH (VWR, Darmstadt, Germany) was dissolved under stirring and under cooling in 85 g deionised water. The anodization was performed under stirring (400 r min^{-1}) using a magnetic stirrer (20 mm stirring bar). The distance between WE and CE was adjusted to 8 mm. A power source (Electra Automatic, Vierssen, Germany) EA-PSI 8360-15T which allows to deliver a constant voltage even at strongly changing current loads was used for the electrochemical oxidation. The voltage was increased in 500 mV steps up to 5.2 V within 10 min. The current varied slightly during the experiment and on average the current was around 5.3 A. The temperature of the electrolyte increased within the first 30 min and reached a value of 323 K. The duration of the surface treatment was varied according to Table 1 in between 300–480 min. After completion of the experiment the WE was taken out of electrolyte and rinsed intensively with tap water for 15 min and afterwards with deionised water for a further 10 min. The used NaOH electrolyte was transferred quantitatively into a plastic bottle and was stored for further analysis. The counter electrode which was covered by a black layer was immersed into 2 M HCl for 12 hours. The acidic solution was stored for further analysis. Prior to the electrochemical characterization the samples were dried under air at ambient temperature. Each of the sample preparation was repeated seven times.

Preparation of the samples – electro oxidation of stainless steel via multicycling technique (sample EloxCycl)

The oxide layer of sample EloxCycl was grown using a repetitive potential multicycling technique within a conventional three electrode set-up consisting of a metal WE, a platinum wire CE (5×4 cm geometric area) and a reversible hydrogen reference electrode (HydroFlex, Gaskatel Gesellschaft für Gassysteme durch Katalyse und Elektrochemie mbH. D-34127 Kassel, Germany). A potentiostat Interface 1000 from Gamry Instruments (Warminster, PA 18974, USA) was employed and interfaced to a personal computer which allows to record all electrochemical data digitally. The WE (anode) was immersed 1.5 cm deep (3.4 cm^2 geometric area), and the CE (cathode) was completely immersed into the electrolyte which was prepared as follows: in a 100 mL glass beaker, 3 g (75 mmol) of NaOH (VWR, Darmstadt) were dissolved under stirring and under cooling in 50 g deionised water. The anodization was performed under stirring (300 r min^{-1}) using a magnetic stirrer (20 mm stirring bar). The RE was placed between the working electrode and the CE. The distance between the WE and the RE was adjusted to 4–5 mm and the distance between the RE and the CE was also adjusted to 4–5 mm. The potential of the WE *vs.* RHE was varied between 0 and 2.25 V. Zero and +2.25 V *vs.* RHE were chosen as limit because of the expected Ni(II)–Ni(III) respectively Ni(III)–Ni(II)

transitions within this potential range. The sweep rate was set to 50 mV s^{-1} and the step size was 20 mV. The experiment was completed after 500 cycles, which corresponds to a total duration of the experiment of 750 min. It turned out that the current peaks are in the range but still below to the current limit of the device (1000 mA). In order to check the reproducibility, the experiment was repeated twice.

Electrochemical measurements. A three electrode set-up was used for all electrochemical measurements. The working electrode (WE) with a total geometry of $100 \times 10 \times 1.5$ mm was constructed from 1.5 mm thick X5CrNi18-10 (304) steel on which an apparent surface area of $\sim$1.5–2 cm^2 was defined by an insulating tape (Kapton tape). The Ni42 sample consists of untreated AISI Ni42 material and was constructed from a disk 50 mm in diameter, 1.5 mm in thickness (Fig. S10, ESI†) on which an apparent surface area of $\sim$2 cm^2 was defined by an insulating tape (Kapton tape). AISI Ni42 was purchased from Schmiedetechnik Faulenbach, Wiehl, Germany. The IrO$_2$–RuO$_2$ sample (10 micrometer layer deposited on titanium; Fig. S7, ESI†) with a total geometry of $100 \times 100 \times 1.5$ mm was purchased from Baoji Changli Special Metal Co, Baoji, China. An electrode area of 2 cm^2 was defined on the plate by Kapton tape. To avoid additional contact resistance the plate was electrically connected *via* a screw. An iron electrode (iron comparison sample) was constructed from iron foil $50 \times 50 \times 2.5$ mm ($>$99.99% purity; Sigma-Aldrich) on which an active area of 1.5 cm^2 was defined by Kapton tape.

A platinum wire electrode (4×5 cm geometric area) was employed as the CE, a reversible hydrogen reference electrode (RHE, HydroFlex, Gaskatel Gesellschaft für Gassysteme durch Katalyse und Elektrochemie mbH. D-34127 Kassel, Germany) was utilized as the reference standard, therefore all voltages are quoted against this reference electrode (RE). For all measurements the RE was placed between the working and the CE. The measurements were performed in a 0.1 M KOH solution (Merck TitriPur). The distance between the WE and the RE was adjusted to 0.4–1 mm and the distance between the RE and the CE was adjusted to 4–5 mm. All electrochemical data were recorded digitally using a Potentiostat Interface 1000 from Gamry Instruments (Warminster, PA 18974, USA), which was interfaced to a personal computer.

Cyclic voltammograms (CV) were recorded in 90 mL 0.1 M KOH in a 100 mL glass beaker under stirring (180 r min^{-1}) using a magnetic stirrer (15 mm stirring bar). The scan rate was set to 20 mV s^{-1} and the step size was 2 mV. The potential was cyclically varied between 1 and 1.7 V *vs.* RHE. No IR compensation was performed whilst recording the CV plots.

Chronopotentiometry scans were conducted at a constant current density of 10 mA cm^{-2} in 1900 mL of 0.1 M KOH in a 2000 mL glass beaker. The scans were recorded under stirring (300 r min^{-1}) using a magnetic stirrer (40 mm stirring bar). As IR compensation *via* standardized software was found to be too strong, *i.e.* lead to anomalous voltage–current behaviour (curves in CV plots) at high potentials, we corrected Ohmic losses within the chronopotentiometry plots manually by subtracting the Ohmic voltage drop from the measured potential

This journal is © The Royal Society of Chemistry 2015

Energy Environ. Sci., 2015, **8**, 2685–2697 | **2695**

Table 3 Key data of the (three electrode) electrochemical set up

Sample	Electrode area (cm^2)	Distance between RE and WE (mm)	Distance between RE and CE (mm)
Elox300	1.5	0.8	5
Elox480	1.5	0.4	4
EloxCycl	1.5	0.6	5
IrO_2–RuO_2	2	0.6	4
Ni42	2	0.6	5
AISI304	2	0.4	5
Iron	1.5	0.6	4

on the basis of a electrolyte (0.1 M KOH) resistance of 50 Ω at 10 mm electrode distance.

Tafel plots. Average voltage values for the Tafel plots of the samples AISI304 (untreated steel), Elox300, Elox480, IrO_2–RuO_2 and Ni42 were derived from 200 second chronopotentiometry scans at current densities of 0.66, 1.33, 2, 2.67, 4, 5.33, 6.67, 8, 10, 13.3, 16.67 and 20 mA cm^{-2}. IR compensation was performed for all plots taking into account the values for electrolyte resistance from Table 3, *i.e.* the geometry of the arrangement of RE, WE and CE taken for recording the chronopontentiometry plots was kept constant.

Spectroscopic analyses

AAS spectroscopy. In total five electro-activation procedures (three times duration 300- and two times duration 480 min) have been investigated to guarantee meaningful data. The results can be taken from Table S3 (ESI†). The CE was, subsequently after finishing the anodization, immersed into 2 M HCl for 4 hours. The electrolyte (7.2 M NaOH) as well as the HCl solution was analyzed *via* Flame Atomic Absorption Spectroscopy (F-AAS, SOLAAR M6, Thermo Scientific, New York, USA) according to DIN 38406-32:2000-05 (Fe), DIN 38406-11:1991-09 (Ni) und DIN EN 1233:1996-08 (Cr). The absorbances were measured with a slit width of 0.2 nm at wavelengths of 248.3 nm (Fe), 232.0 nm (Ni) and 357.9 nm (Cr). The sodium hydroxide-containing electrolyte solutions were due to the high salinity (total dissolved solids (TDS) > 300 g L^{-1}) first diluted by a factor of 10 with deionised water and then stabilized with hydrochloric acid (34 wt%; VWR, Darmstadt, Germany) until pH 5 was reached. Since after diluting the electrolyte, TDS still exceeded the maximum value of 15 g L^{-1} for interference-free measurements, the standard addition method based on DIN 32633 was chosen for the measurement. The hydrochloric acid solutions were also diluted depending on the element content with deionised water. Again, the standard addition method was used for determination of element concentrations due to increased TDS levels. The correlation coefficient r of the linear regression to determine the element concentrations in the sample solutions were $9.9532 \times 10^{-1} \leq r \leq 9.9999 \times 10^{-1}$, error sums of squares (rss) were $2.2299 \times 10^{-5} \leq \text{rss} \leq 2.0751$.

XPS spectroscopy. XPS measurements were performed using a PHI 5600ci multitechnique spectrometer equipped with a monochromatic Al Kα source with 0.3 eV full width at half-maximum. The overall resolution of the spectrometer is 1.5% of the pass energy of the analyser, 0.7 eV in the present case.

The measurements were recorded with the sample at room temperature. The spectra were calibrated with a corresponding measurement of the Au 4f$_{7/2}$ level (84.0 eV) of a gold foil.

As to the evaluation of the cationic composition of the samples, a standard Shirley background is subtracted from all spectra. The relative elemental Cr, Fe, and Ni concentration were determined using the PHI sensitivity factors (see Table 2) included in the PHI Multipak program package. Please note: measurements performed before and after carrying out the chronopotentiometry scans (duration: 50 000 s) showed the same value.

Electron microscopic experiments – microstructure of the oxide layer. The surface morphology of the layers was characterized by a Zeiss EVO MA 10 Scanning Electron Microscopy (SEM) equipped with an Oxford Inca Energy 250 Energy-dispersive X-ray spectroscopy (EDS) device.

AFM and STM experiments. AFM measurements are done in contact mode on a Quesant Instrument Corp. model Q250 equipment using a NSC16 type tip. The cantilevers had nominal lengths of ± 5 µm, force constants, N m^{-1} 45 of (25–60), and resonance frequencies 170 (150–190) range. The tip radius was <10 nm. The AFM images were processed by the free software package Gwydion. STM imaging was performed on an EasyScanII Nanosurf (Switzerland) instrument at 22 °C using typically 0.050 V bias voltages and 1 nA tunnelling current. The STM tips were cut from Pt/Ir wire (0.25 mm, Schaefer Technologie GmbH, Langen, Germany).

References

1 M. G. Walter, E. L. Warren, J. R. McKone, S. W. Boettcher, Q. Mi, E. A. Santori and N. S. Lewis, *Chem. Rev.*, 2010, **110**, 6446.

2 T. R. Cook, D. K. Dogutan, S. Y. Reece, Y. Surendranath, T. S. Teets and D. G. Nocera, *Chem. Rev.*, 2010, **11**(110), 6474.

3 A. J. Bard and M. A. Fox, *Acc. Chem. Res.*, 1995, **28**, 141.

4 Y. Lee, J. Suntivich, K. J. May, E. E. Perry and Y. Shao-Horn, *J. Phys. Chem. Lett.*, 2012, **3**(3), 399.

5 Y. Gorlin and T. F. Jaramillo, *J. Am. Chem. Soc.*, 2010, **132**, 13612.

6 S. Trasatti, *Electrochim. Acta*, 1984, **29**, 1503.

7 S. Trasatti, *Electrochim. Acta*, 1987, **32**, 369.

8 S. Trasatti, *Electrochim. Acta*, 2000, **45**, 2377.

9 V. Petrykin, K. Macounova, O. A. Shlyakhtin and P. Krtil, *Angew. Chem., Int. Ed.*, 2010, **49**, 4813.

10 T. Nakagawa, C. A. Beasley and R. W. Murray, *J. Phys. Chem. C*, 2009, **113**, 12958.

11 Y. Zhao, E. A. Hernandez-Pagan, N. M. Vargas-Barbosa, J. L. Dysart and T. E. Mallouk, *J. Phys. Chem. Lett.*, 2011, **2**, 402.

12 M. E. G. Lyons and M. P. Brandon, *J. Electroanal. Chem.*, 2010, **641**, 119.

13 M. E. G. Lyons and S. Floquet, *Phys. Chem. Chem. Phys.*, 2011, **13**, 5314.

14 M. S. El-Deab, M. I. Awad, A. M. Mohammad and T. Ohsaka, *Electrochem. Commun.*, 2007, **9**, 2082.

15 F. Jiao and H. Frei, *Chem. Commun.*, 2010, **46**, 2920.

16 M. M. Najafpour, *Dalton Trans.*, 2011, **40**, 3805.

17 F. Zhou, A. Izgorodin, R. K. Hocking, L. Spiccia and D. R. MacFarlane, *Adv. Energy Mater.*, 2012, **2**, 1013.

18 S. I. Cordoba, R. E. Carbonio, M. Lopez Teijelo and V. A. Macagno, *Electrochim. Acta*, 1987, **32**(5), 749.

19 L. Trotochaud, J. K. Ranney, K. N. Williams and S. W. Boettcher, *J. Am. Chem. Soc.*, 2012, **134**, 17253.

20 M. W. Louie and A. T. Bell, *J. Am. Chem. Soc.*, 2013, **135**, 12329.

21 Y. Qiu, L. Xin and W. Li, *Langmuir*, 2014, **30**, 7893.

22 L. Trotochaud, S. L. Young, J. K. Rannes and S. W. Boettcher, *J. Am. Chem. Soc.*, 2014, **136**, 6744.

23 N. Sato and G. Okamoto, *Electrochim. Acta*, 1965, **10**, 495.

24 M. H. Miles, G. Kissel, P. W. T. Lu and S. Srinivasan, *J. Electrochem. Soc.*, 1976, **123**, 332.

25 J. Cerny and K. Micka, *J. Power Sources*, 1989, **25**, 111.

26 M. E. G. Lyons and R. E. Doyle, *Int. J. Electrochem. Sci.*, 2011, **6**, 5710.

27 K. C. Leonard, M. I. Tejedor-Anderson and M. A. Anderson, *Int. J. Hydrogen Energy*, 2012, **37**, 18654.

28 F. Moureaux, P. Stevens, G. Toussaint and M. Chatenet, *J. Power Sources*, 2013, **229**, 123.

29 M. E. G. Lyons and R. L. Doyle, *Int. J. Electrochem. Sci.*, 2012, **7**, 9488.

30 M. E. G. Lyons and L. D. Burke, *J. Electroanal. Chem.*, 1984, **170**, 377.

31 K. Lian, S. J. Thorpe and D. W. Kirk, *Electrochim. Acta*, 1992, **37**(1), 169.

32 T. Kessler, W. E. Triaca and A. J. Arvia, *J. Appl. Electrochem.*, 1994, **24**, 310.

33 W. D. Chemelewski, H.-C. Lee, J.-F. Lin, A. J. Bard and C. B. Mullins, *J. Am. Chem. Soc.*, 2014, **136**, 2843.

34 J. O. Bockris and T. Otagawa, *J. Electrochem. Soc.*, 1984, **131**, 290.

35 A. C. C. Tseung and S. Jasem, *Electrochim. Acta*, 1977, **22**, 31.

36 C. R. Davidson, K. Kissel and S. Srinivasan, *J. Electroanal. Chem.*, 1982, **132**, 129.

37 J. Suntivich, K. J. May, H. A. Gasteiger, J. B. Goodenough and Y. S. Horn, *Science*, 2011, **334**, 1383.

38 A. Grimaud, K. J. May, C. E. Carlton, Y.-L. Lee, M. Risch, W. T. Hong, J. Zhou and Y. Shao-Horn, *Nat. Commun.*, 2013, **4**, 2439.

39 S. Chen and S.-Z. Qiao, *ACS Nano*, 2013, **7**(11), 10190.

40 W. Zhou, X.-J. Wu, X. Cao, X. Huang, C. Tan, J. Tian, H. Liu, J. Wang and H. Zhang, *Energy Environ. Sci.*, 2013, **6**, 2921.

41 V. K. V. Prasad Srirapu, C. Shekhar Sharma, R. Awasthi, R. Nath Singh and A. S. Kumar Sinha, *Phys. Chem. Chem. Phys.*, 2014, **16**, 7385.

42 H.-C. Chien, W.-Y. Cheng, Y.-H. Wang, T.-Y. Wie and S.-Y. Lu, *J. Mater. Chem.*, 2011, **21**, 18180.

43 R. F. Scarr, *J. Electrochem. Soc.: Electrochem. Sci.*, 1969, **116**, 1531.

44 L. D. Burke and T. A. M. Twomey, *J. Electroanal. Chem.*, 1984, **162**, 101.

45 M. R. Gennero De Chivalo and A. C. Chivalo, *Electrochim. Acta*, 1988, **33**, 825.

46 S. Uhlenbrock, C. Scharfschwerdt, M. Neumann, G. Illing and H. J. Freund, *J. Phys.: Condens. Matter*, 1992, **4**, 7973.

47 M. C. Biesinger, B. P. Payne, A. P. Grosvenor, L. W. M. Lau, A. R. Gerson and R. St. C. Smart, *Appl. Surf. Sci.*, 2011, **257**, 2717.

48 A. Cocijan, C. Donik and M. Jenko, *Corros. Sci.*, 2007, 2083.

49 A. P. Grosvenor, B. A. Kobe, M. C. Biesinger and N. S. McIntrye, *Surf. Interface Anal.*, 2004, **36**, 1564.

50 C. Klewe, M. Meinert, A. Boehnke, K. Kuepper, E. Arenholz, A. Gupta, J. M. Schmalhorst, T. Kuschel and G. Reiss, *J. Appl. Phys.*, 2014, **115**, 123903.

51 H. Schäfer, C. Hess, H. Tobergte, A. Volf, S. Ichilmann, H. Eickmeier, M. Steinhart, B. Voss, N. Kashaev, J. Nordmann and W. Akram, *Small*, 2015, **11**, 931.

52 M. Haase and H. Schäfer, *Angew. Chem., Int. Ed.*, 2011, **50**, 5808.

53 P. Ptacek, H. Schäfer, K. Kömpe and M. Haase, *Cryst. Growth Des.*, 2010, **10**(5), 2434.

54 H. Bode, K. Dehmelt and J. Witte, *Electrochim. Acta*, 1966, **11**, 1079.

55 J. Rossmeisl, A. Logadottir and J. K. Nørskov, *Chem. Phys.*, 2005, **319**, 178.

56 J. Rossmeisl, Z.-W. Qu, H. Zhu, G.-J. Kroes and J. K. Nørskov, *J. Electroanal. Chem.*, 2007, **607**, 83.

57 A. S. Anindita and R. N. Singh, *Int. J. Hydrogen Energy*, 2010, **35**, 3243.

58 R. N. Singh, J. P. Singh, B. Lal, M. J. K. Thomas and S. Bera, *Electrochim. Acta*, 2006, **51**, 5515.

59 R. N. Singh, J. P. Singh and A. Singh, *Int. J. Hydrogen Energy*, 2008, **33**, 4260.

60 R. N. Singh, N. K. Singh, J. P. Singh, G. Balaji and N. S. Gajbhiye, *Int. J. Hydrogen Energy*, 2006, **31**, 701.

61 H. Schäfer, S. M. Beladi-Mousavi, L. Walder, J. Wollschläger, O. Kuschel, S. Ichilmann, S. Sadaf, M. Steinhart, K. Küpper and L. Schneider, *ACS Catal.*, 2015, **5**, 2671.

62 W. O'Grady, C. Iwakura, J. Huang and E. Yeager, in *Proceedings of the Symposium on Electrocatalysis*, ed. M. W. Breiter, The Electrochemical Society Inc., Pennington, NJ, 1974, p. 286.

63 R. E. Meyer, *J. Electrochem. Soc.*, 1960, **107**, 847.

64 S. L. Medway, C. A. Lucas, A. Kowal, R. J. Nichols and D. Johnson, *J. Electroanal. Chem.*, 2006, **587**, 172.

65 C. B. Lee, B. S. Kang, M. J. Lee, S. E. Ahn, G. Stefanovich, W. X. Xianyu, K. H. Kim, J. H. Hur, H. X. Yin, Y. Park, I. K. Yoo, J.-B. Park and B. H. Park, *Appl. Phys. Lett.*, 2007, **91**, 082104.

66 X. L. Zou, S. L. Gu, H. W. Cheng, X. G. Lu, Z. F. Zhou, C. H. Li and W. Z. Ding, *J. Electrochem. Soc.*, 2015, **162**, D49.

67 N. Wang, T. Hang, S. Shanmugan and M. Li, *CrystEngComm*, 2014, **16**, 6937.

68 K. Ngamlerdpokin and N. Tantavichet, *Int. J. Hydrogen Energy*, 2014, **39**, 2505.

69 M. C. Biesinger, L. W. M. Lau, A. R. Gerson and R. S. C. Smart, *Phys. Chem. Chem. Phys.*, 2012, **14**, 2434.

This journal is © The Royal Society of Chemistry 2015

Energy Environ. Sci., 2015, **8**, 2685–2697 | **2697**